ADVANCING EARTH AND SPACE SCIENCES

Geophysical Research Letters

RESEARCH LETTER
10.1029/2024GL111708

L-Band InSAR Snow Water Equivalent Retrieval Uncertainty Increases With Forest Cover Fraction

R. Bonnell[1], **K. Elder**[2], **D. McGrath**[1], **H. P. Marshall**[3], **B. Starr**[2], **N. Adebisi**[3], **R. T. Palomaki**[4], **and Z. Hoppinen**[3,5]

[1]Department of Geosciences, Colorado State University, Fort Collins, CO, USA, [2]Rocky Mountain Research Station, USDA Forest Service, Fort Collins, CO, USA, [3]Department of Geosciences, Boise State University, Boise, ID, USA, [4]Institute of Arctic and Alpine Research, University of Colorado, Boulder, CO, USA, [5]U.S. Army Cold Regions Research and Engineering Laboratory, Hanover, NH, USA

K. Elder and D. McGrath contributed equally to this work

Key Points:

- We evaluated L-band interferometry for snowpack monitoring in a montane forest in Colorado
- Retrievals of changes in snow water equivalent from L-band interferometry were accurate and unbiased in forest cover fractions <0.40
- Despite limitations, L-band interferometry represents a promising path toward global snowpack monitoring

Supporting Information:

Supporting Information may be found in the online version of this article.

Correspondence to:

R. Bonnell,
rbonnell@colostate.edu;
rbonnell@usgs.gov

Citation:

Bonnell, R., Elder, K., McGrath, D., Marshall, H. P., Starr, B., Adebisi, N., et al. (2024). L-band InSAR snow water equivalent retrieval uncertainty increases with forest cover fraction. *Geophysical Research Letters*, *51*, e2024GL111708. https://doi.org/10.1029/2024GL111708

Received 31 JUL 2024
Accepted 3 DEC 2024

Author Contributions:

Conceptualization: R. Bonnell, K. Elder, D. McGrath, H. P. Marshall
Data curation: R. Bonnell, K. Elder, B. Starr, N. Adebisi
Formal analysis: R. Bonnell, R. T. Palomaki, Z. Hoppinen
Funding acquisition: R. Bonnell, K. Elder, D. McGrath, H. P. Marshall
Investigation: K. Elder, B. Starr
Methodology: R. Bonnell, K. Elder, D. McGrath, H. P. Marshall
Visualization: R. Bonnell
Writing – original draft: R. Bonnell

Abstract There is a pressing need for global monitoring of snow water equivalent (SWE) at high spatiotemporal resolution, and L-band (1–2 GHz) interferometric synthetic aperture radar (InSAR) holds promise. However, the technique has not seen extensive evaluation in forests. We evaluated this technique across varying forest canopy conditions using eight InSAR pairs collected at the Fraser Experimental Forest, Colorado, USA by NASA UAVSAR during the 10-week NASA SnowEx 2021 Campaign. Compared with in situ measurements, we found root mean squared errors (RMSEs) of 14–17 mm for SWE changes in forest cover fractions (FCF) < 0.40, but RMSEs increased to 33–40 mm at FCF > 0.50. Statistical distributions between normalized lidar snow depths and normalized UAVSAR SWE were similar at FCF < 0.5, but diverged at FCF > 0.50. Thus, the upcoming NISAR L-band satellite has strong potential for global snowpack monitoring, including below sparse to moderate forest cover.

Plain Language Summary Monitoring the amount of water stored in seasonal snowpacks is essential for water resource management, but it remains challenging, particularly in mountain and forest environments. Satellite radar techniques may provide a viable path forward for snowpack monitoring, particularly at longer radar wavelengths (>20 cm) such as the radar used for the upcoming NASA-ISRO SAR satellite mission. At these longer wavelengths, the radar signal can penetrate forest canopy, but the canopy interferes with the signal and may reduce the accuracy of the radar snowpack measurement. We examined the influence of forest cover on airborne radar measurements of the snowpack in the Fraser Experimental Forest, Colorado, USA and observed errors that increased with greater forest cover. Notably, the radar measurements were accurate for sparse to moderately dense forest covers. The radar snowpack measurements reproduced elevational trends observed in lidar-measured snow depths, but we identified snowpack measurement errors that correlated with oblique radar viewing geometries. Considering these limitations, we conclude that the NASA-ISRO SAR satellite mission represents a promising path toward global snowpack monitoring.

1. Introduction

The monitoring of seasonal snowpacks is critical for understanding ecosystems (Gleason et al., 2021; Pedersen et al., 2021), drought forecasting (Livneh & Badger, 2020), and managing snowmelt runoff, an important resource for billions of people (Barnett et al., 2005; Sturm et al., 2017). The remote sensing of snow water equivalent (SWE), one of the defining snow hydrologic variables, is highly prioritized, with an absolute SWE accuracy goal of 30 mm at high spatiotemporal resolution (<500 m; ~weekly; NASEM, 2018). However, current snowpack monitoring is insufficient, particularly within mountains, where complex topography, montane forests, and highly variable snowpack distributions present significant challenges for remote sensing (Dozier et al., 2016). Methods for snow depth/SWE retrievals are in development, but snowpack measurements within forests remain a significant challenge (Hu et al., 2023; Lievens et al., 2019; Oveisgharan et al., 2024).

The retrieval of SWE below forest canopy is critical because ~33% of Earth's seasonal snow cover is found in forested environments (NASA SnowEx, 2024). In the western contiguous USA, an estimated 70% of the seasonal snow-covered area is forested and almost entirely contained within mountain environments (Bourgoin et al., 2023; Moore et al., 2012; Wrzesien et al., 2018) which generate 70% of region-wide runoff (Li et al., 2017). In these complex environments, methods using satellite-based synthetic aperture radar (SAR) are front-runners for measuring SWE at the targeted spatiotemporal resolution (NASEM, 2018).

Writing – review & editing: R. Bonnell, K. Elder, D. McGrath, R. T. Palomaki, Z. Hoppinen

SARs are side-looking radars that transmit a signal and record the amplitude and phase of the backscattered return. Radar waves <18 GHz are transmissible through snow, and the primary reflecting boundary occurs at interfaces with strongly contrasting dielectric permittivities (e.g., the snow-ground interface; Deeb et al., 2011). SAR platforms have high spatial resolution and repeat cycles of 6–14 days. Although the radar signal interacts with the forest canopy, SAR at lower frequencies (e.g., L-band, 1–2 GHz, 15–30 cm wavelength) may be capable of sub-canopy SWE retrievals because the radar wave can penetrate the canopy. Here, we discuss the interferometric SAR (InSAR) approach for measuring a change in SWE (ΔSWE) from the phase-change between two SAR acquisitions (Guneriussen et al., 2001; Text S2.1 in Supporting Information S1). This approach for SWE retrievals has been implemented using tower-based radars (e.g., Ruiz et al., 2022), satellites (e.g., Oveisgharan et al., 2024), and for airborne SARs (e.g., NASA Uninhabited Aerial Vehicle SAR or UAVSAR) across several frequency bands. Relevant InSAR SWE retrieval studies are listed in Table S1 in Supporting Information S1. Compared with higher frequency InSAR approaches, L-band InSAR is advantageous because coherence, a measure of similarity between two signals, can be maintained for longer temporal baselines (e.g., 12-day; Ruiz et al., 2022). However, the technique is likely not applicable in wet snow and high uncertainty is expected below forest cover (e.g., Ruiz et al., 2022).

Here, we evaluate eight L-band InSAR pairs collected from the UAVSAR platform as part of the SnowEx 2021 Time Series Campaign at the Fraser Experimental Forest (FEF), Colorado, USA. In situ measurements were collected across a range of elevations (2,700–3,400 m) in meadows and lodgepole pine/spruce-fir forests (Text S1.1 in Supporting Information S1). Snow-on/off airborne lidar scans were collected in March/September 2021 to measure spatially distributed vegetation heights and snow depths near the end of the UAVSAR campaign. Our study examines the applicability and limitations of this method in montane forests by addressing two key questions.

1. What is the accuracy of L-band InSAR ΔSWE retrievals from single interferometric pairs in both forested and open environments based on field measurements?
2. Based on spatially expansive lidar snow depths, what are the uncertainties of an InSAR ΔSWE time series across elevations, forest cover fractions, and SAR incidence angles?

Our work informs potential applications and limitations of the technique in forests for the upcoming L-band NISAR satellite mission (planned 2025 launch). Because data sets collected by NISAR will be publicly available at high spatiotemporal resolution (80 m, 12-day revisit), this technique may offer a clear path toward open-access SWE retrievals in the world's water towers (Immerzeel et al., 2020).

2. NASA SnowEx at Fraser Experimental Forest

The NASA SnowEx 2021 Time Series campaign was implemented at seven field sites across the western USA (Marshall et al., 2020). The campaign emphasized acquisitions from UAVSAR, a quad-polarized L-band (1.26 GHz center frequency, 0.24 m wavelength, 80 MHz bandwidth) left-looking SAR with InSAR capabilities. Eight InSAR pairs with a northwest heading (052°) and four pairs from the reverse heading (233°) were collected over FEF in Colorado (Figure 1a). UAVSAR flew at an altitude of ∼12.5 km AGL approximately weekly from 15 January to 22 March 2021.

FEF has a dry continental snow climate (Trujillo & Molotch, 2014) with a 12-year median peak SWE of 569 mm recorded by the Fool Creek SNOTEL station (3,400 m elevation). During UAVSAR flights (±1 day), probed snow depths and snow pit measurements of depth, density, temperature, relative permittivity, and stratigraphy were collected at three field sites: Headquarters (HQ; 0.3 km^2), St. Louis Creek (StL; 1.4 km^2), and Fool Creek (FC; 1.4 km^2; Figures 1d–1f). The Fool Creek SNOTEL station is near FC and records snow depth, SWE, and air temperature at hourly intervals. FEF has a large elevation range (∼1,000 m) with communities of lodgepole pine (*Pinus contorta*) and aspen (*Populus tremuloides*) at lower elevations and Engelmann spruce (*Picea engelmannii*) and subalpine fir (*Abies lasiocarpa*) at higher elevations (Huckaby & Moir, 1998). Of the three sites, FC is located at the highest elevation and has the highest average forest cover fraction (∼3,200 m; 0.62 FCF), whereas both HQ and StL have similar site-wide metrics and are located at relatively lower elevations with lower FCF (∼2,700 m; 0.20 FCF). UAVSAR acquisitions were performed before the snowmelt period (∼1 April for HQ, ∼14 May for FC). Snow-on (19 March 2021; ∼78% of peak SWE at SNOTEL) and snow-free (18 September 2021) lidar scans were collected by NV5 Geospatial to measure spatially distributed snow depths and vegetation heights (Adebisi

10.1029/2024GL111708

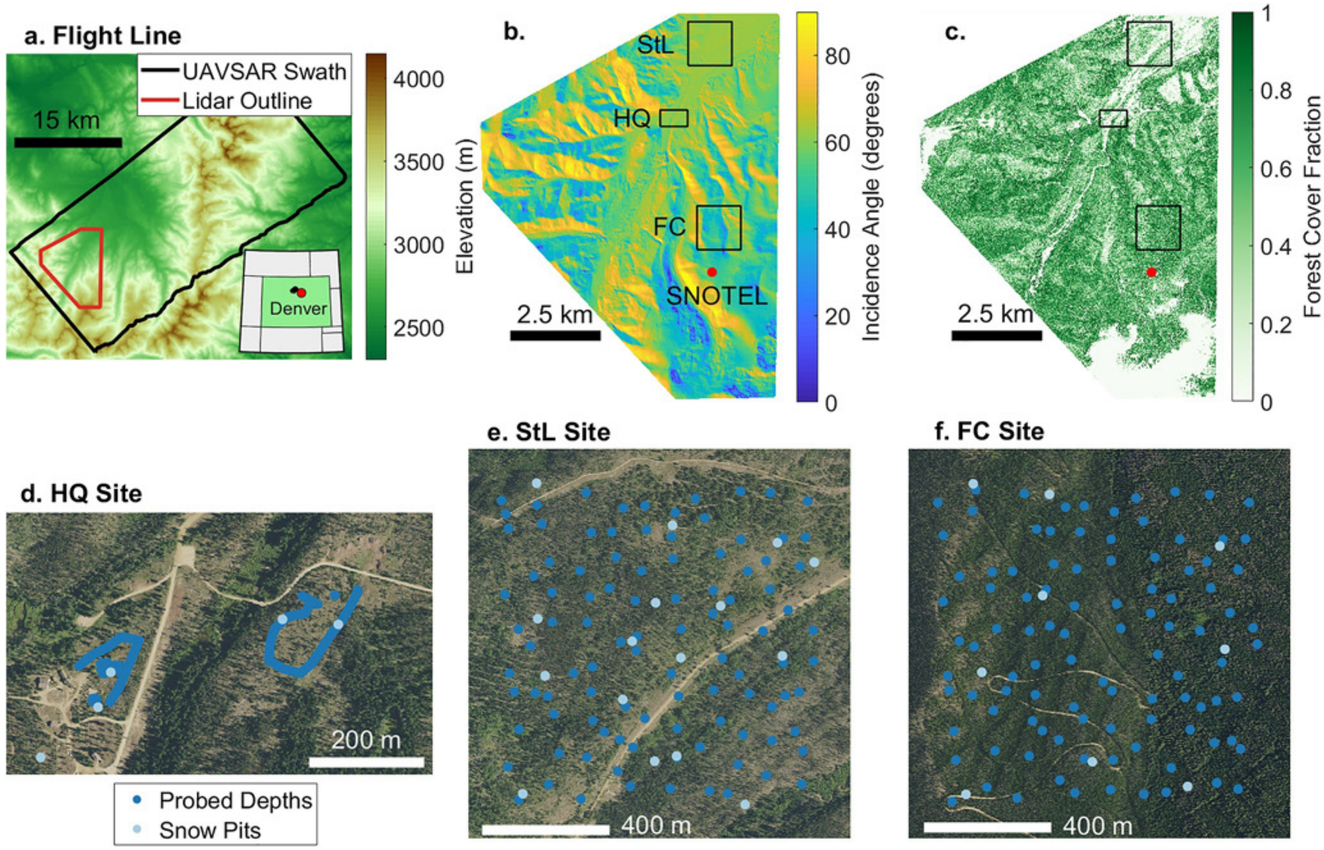

Figure 1. (a) Copernicus 30 m DEM with Fraser, CO UAVSAR swath and inset map of Colorado. Study area showing (b) UAVSAR local incidence angles (052° heading) derived from the lidar DEM and (c) FCF derived from lidar vegetation heights. NAIP imagery with locations of depth probe and snow pit measurements at the (d) HQ, (e) StL, and (f) FC field sites.

et al., 2022b, 2022c). In situ sampling strategies are described in Text S1 in Supporting Information S1 and UAVSAR flight dates and field survey dates/observations are available in Table S2 in Supporting Information S1.

3. Methods

3.1. Processing UAVSAR Data Sets

We present detailed methods for the ΔSWE calculation and the polarimetric decomposition from UAVSAR data sets in Text S2 in Supporting Information S1. Here, we provide a summary of the data sets and processing flow. UAVSAR data sets were collected and processed to ~6 m resolution by the UAVSAR team. We accessed nearest temporal neighbor InSAR pair data sets (ground projected unwrapped interferograms and coherence products) and the POLSAR data sets (ground projected σ^0 products) via the Alaska Satellite Facility (NASA UAVSAR, 2021) through uavsar_pytools (Hoppinen & Tarricone, 2022). We performed a polarimetric decomposition to better understand how the scattering characteristics vary by forest cover (Text S2.4 in Supporting Information S1). We removed an atmospheric phase ramp through linear regression from both headings of the 3–10 March InSAR pairs (Text S2.2 in Supporting Information S1). Regression slope parameters were negative for both headings, although the values differed slightly due to contrasting viewing geometries. We determined that liquid water content was either absent or <1 vol. % during UAVSAR flights based on snow pit measurements (Figure S3; Text S2.3 in Supporting Information S1), but melt may have occurred in canopy-intercepted snow, which was present during March surveys (Figure S4 in Supporting Information S1). Phase calibration for the unwrapped interferograms was calculated as the difference between phase-change estimated from ΔSWE at an HQ snow pit with high coherence (>0.6) and the median phase-change from the 3 × 3 pixel grid around the snow pit (Table S3 in Supporting Information S1). Two intervals used calibrated phase based on the HQ interval board due to missing snow pit data. We inverted unwrapped interferograms for snow depth change (Guneriussen

10.1029/2024GL111708

et al., 2001) using relative permittivity estimated from the upper 10 cm of snow pit-measured densities (Kovacs et al., 1995) and the local incidence angle calculated from the lidar DEM (Adebisi et al., 2022a). Snow depth change was converted to ΔSWE using the average of all surface (upper 10 cm) snow pit-measured densities collected on the lattermost date of each InSAR pair (Text S2.1 in Supporting Information S1). Based on previous studies, the assumed density likely contributes <7% to ΔSWE uncertainty (Hoppinen et al., 2024; Leinss et al., 2015). ΔSWE was calculated for all four polarizations (Text S2.1 in Supporting Information S1), but we present only the VV polarization in the main text, except for 3–23 February, which used the VH polarization due to phase unwrapping errors in the other polarizations.

3.2. Evaluating UAVSAR With in Situ Measurements

We grouped in situ measurements into two categories: SWE measured directly from snow pits, the SNOTEL station, and the HQ interval board as SWE_{sp} and SWE converted from probed snow depths as SWE_{ds}. We estimated SWE_{ds} by multiplying snow depths by the average bulk snow density from the appropriate field site. For 3–17 March, only probed depths were collected at StL and we converted StL probed depths to SWE using the average HQ bulk snow density. HQ offers a reasonable approximation for snow densities at StL because both sites have similar elevations, FCF, and energy balances, and differences in average densities between HQ and StL on coinciding dates were <5 kg m^{-3}.

We calculated UAVSAR ΔSWE over a 3 × 3 pixel (∼18 × ∼18 m) grid surrounding each SWE_{sp} measurement to reduce uncertainty imposed by the snow pit disturbance. For SWE_{ds}, only one coincident UAVSAR ΔSWE pixel was compared with the ΔSWE_{ds} measurement. We calculated Pearson's correlation coefficient (r) and the root mean squared error (RMSE) for ΔSWE_{sp} and ΔSWE_{ds}. Comparisons were binned by FCF, coherence, and temporal baseline to evaluate the influence of these parameters upon UAVSAR ΔSWE retrieval accuracy. Finally, median ΔSWE_{sp} and ΔSWE_{ds} and median UAVSAR ΔSWE measurements were summed for each interval at each of the three field sites and compared. The starting SWE value for each field site was the median in situ SWE for the site on the first date of field observations. The time series at FC was primarily calculated from the SNOTEL station, because only two surveys were performed at this site (Table S2 in Supporting Information S1).

3.3. Evaluating UAVSAR With Lidar Snow Depths

We resampled the 0.5 m 19 March lidar snow depth data set (Adebisi et al., 2022b) to the ∼6 m UAVSAR grid and evaluated the lidar snow depth accuracy against probed snow depths collected on 17 March (RMSE = 0.22 m; Figure S5 in Supporting Information S1). We integrated UAVSAR ΔSWE by summing the 052° heading ΔSWE products from 15 January to 22 March. The lidar snow depths represent absolute snow depths at the end of the UAVSAR campaign and are, therefore, not directly comparable to the integrated UAVSAR SWE, which represents the accumulated snow mass during the 10-week campaign. However, given the absence of distributed density measurements and because SWE variability is primarily controlled by snow depth variability (Jonas et al., 2009), we normalized the lidar snow depths and cumulative UAVSAR SWE (e.g., Palomaki & Sproles, 2023) using the z-score method to compare the spatial distributions across varying FCF, elevation, UAVSAR incidence angle, and median coherence to define L-band InSAR limitations across a larger spatial scale.

3.4. Calculating FCF

We used 0.5 m resolution lidar vegetation heights (Adebisi et al., 2022c) to generate a binary canopy cover data set, using a 2 m threshold to distinguish canopy from brush. FCF was calculated as the fraction of 0.5 m pixels identified as forest canopy within a 10 m radius for in situ measurements and per ∼6 m pixel for the UAVSAR versus lidar analysis (Figure 1c).

4. Results

4.1. UAVSAR ΔSWE Retrievals

The 052° and 233° UAVSAR ΔSWE retrievals are presented in Figure 2 and Figure S6 in Supporting Information S1. The largest SWE accumulation occurred for the 3–23 February (46 ± 17 mm) interval, whereas the 3–

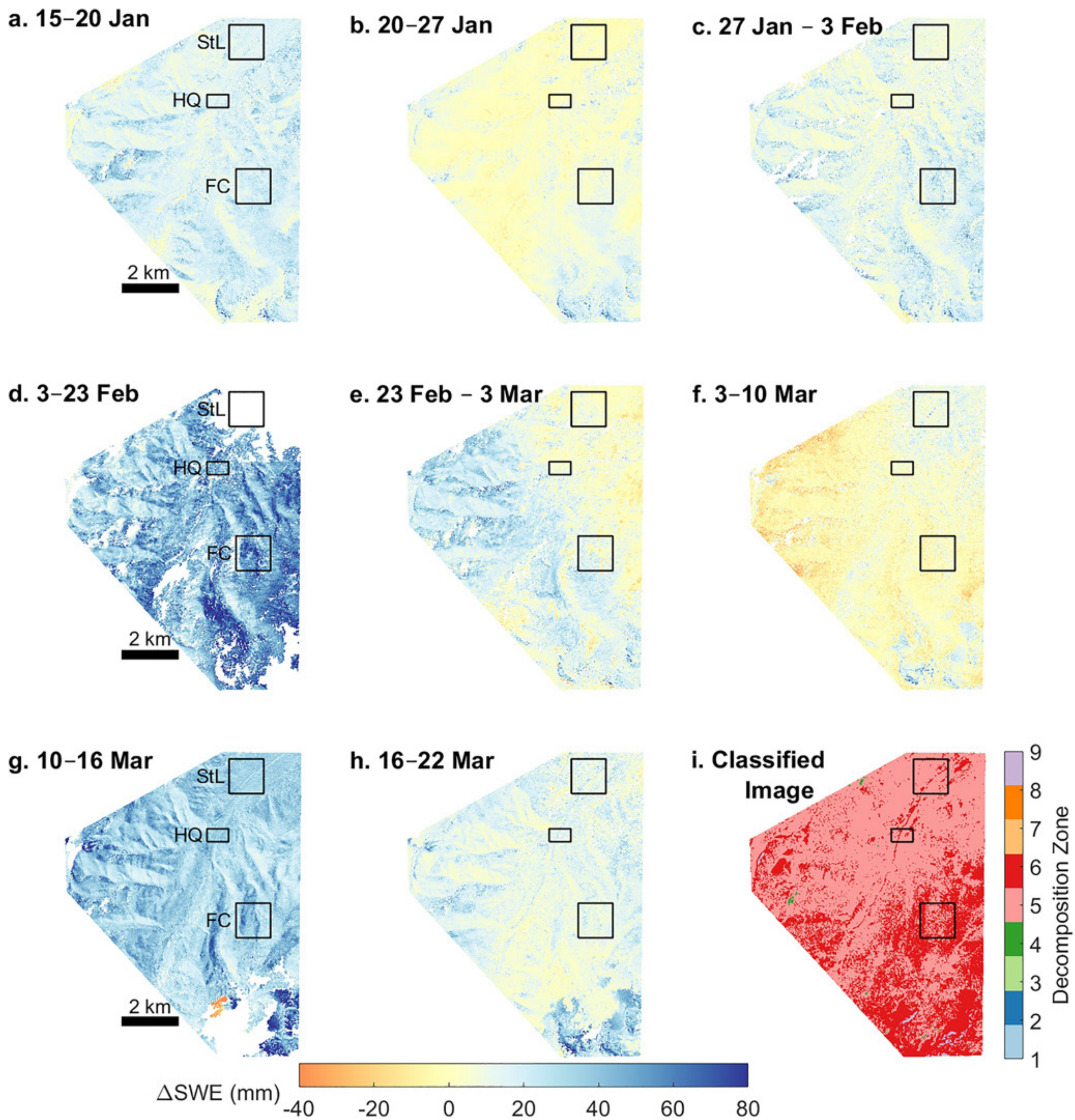

Figure 2. (a–c), (e–h) VV and (d) VH UAVSAR ΔSWE retrievals at the study site for each 052° InSAR pair. Field sites are outlined in black. White denotes missing data due to phase unwrapping issues. (i) Classified image from polarimetric decomposition. Zones identified via Cloude and Pottier (1997).

10 March interval (0 ± 10 mm) observed negligible gains/losses in SWE. ΔSWE retrieval means and standard deviations were similar between the 052° and 233° headings and across all polarizations (Figure 2, Figure S6; Table S4 in Supporting Information S1), but Pearson's correlation coefficients were higher between the two co-polarized channels than between VV and either of the cross-polarized channels (Figure S7 in Supporting Information S1).

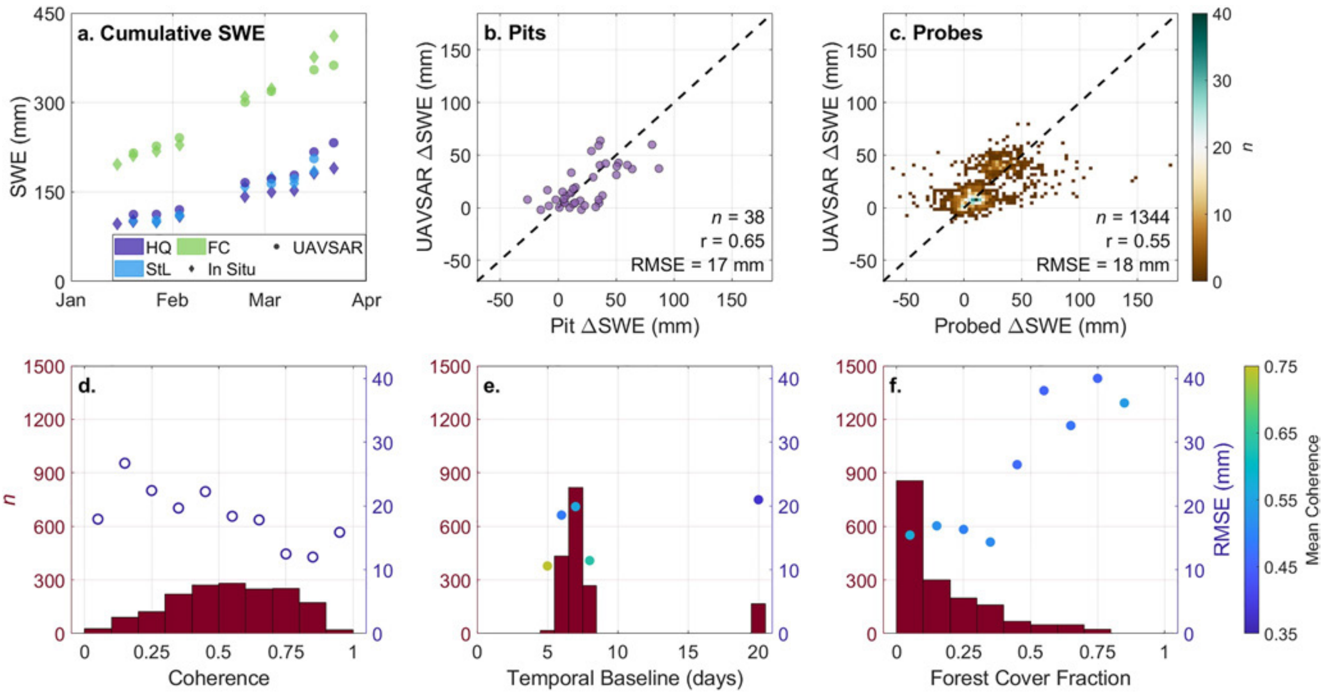

Figure 3. (a) Median SWE measured/estimated from in situ measurements compared with median integrated 052° heading UAVSAR SWE for each field site. UAVSAR ΔSWE evaluated against (b) ΔSWE_{sp} measurements and (c) ΔSWE_{ds} measurements. Histograms and RMSE for each histogram bin for (d) coherence, (e) temporal baseline, and (f) forest cover fraction. Points on e and f are colored by the mean coherence calculated within the bin.

The polarimetric decomposition resulted in four scattering categories for FEF (Figure 2i, Figure S11 in Supporting Information S1). Smooth surface scatter (Zone 9) is exclusively observed above treeline. Smooth surface scatter with some canopy scatter (Zone 6), volume scattering from vegetation (Zone 5), and double bounce (Zone 4), potentially from large trees, are observed in the remainder of the scene. 95% of the study site is classified as medium entropy, a metric of signal depolarization, and 5% is classified as low entropy, indicating that depolarization occurs even for unforested areas. The overall mean anisotropy, used to describe the number of backscattering interfaces, is 0.35 with <1% of values >0.5, indicating a low likelihood of more than one dominant backscattering interface in the forests.

4.2. UAVSAR Versus in Situ Observations

For the 052° heading, cumulative average UAVSAR SWE was within ±12% of the average in situ SWE at StL and FC for all InSAR intervals, whereas UAVSAR at HQ overestimated SWE by up to 22% by the end of the campaign (Figure 3a). The largest divergence between UAVSAR and in situ measurements occurred during the 10–16 and 16–22 March intervals, where UAVSAR overestimated SWE at the HQ and StL sites and underestimated SWE at the FC site. UAVSAR ΔSWE yielded similar comparisons with coincident ΔSWE_{sp} (RMSE = 17 mm, $r = 0.65$; Figure 3b) and ΔSWE_{ds} (RMSE = 18 mm, $r = 0.55$; Figure 3c). For reference, the overall RMSE and r for the VV 233° heading was 20 mm and 0.52 (Figure S8 in Supporting Information S1). RMSE for the 052° heading InSAR pairs, compared against ΔSWE_{ds}, varied from 8 mm (20–27 January) to 28 mm (10–16 March) and overall RMSEs ranged from 18 to 22 mm across the four polarizations and two headings (Tables S5, S6 in Supporting Information S1).

The RMSE increased by a factor of two from high coherence (0.70–0.90) to low coherence (0.10–0.30; Figure 3d), but RMSE for 7-day and 20-day temporal baselines were similar (Figures 3d and 3e). RMSE increased from ∼15 mm at FCF < 0.40 to 26 mm for FCF between 0.40 and 0.50. RMSE approached 40 mm for FCF > 0.50. UAVSAR ΔSWE retrievals yielded negative biases of −22 to −16 mm for FCF > 0.5 (Figure S9c in Supporting Information S1).

10.1029/2024GL111708

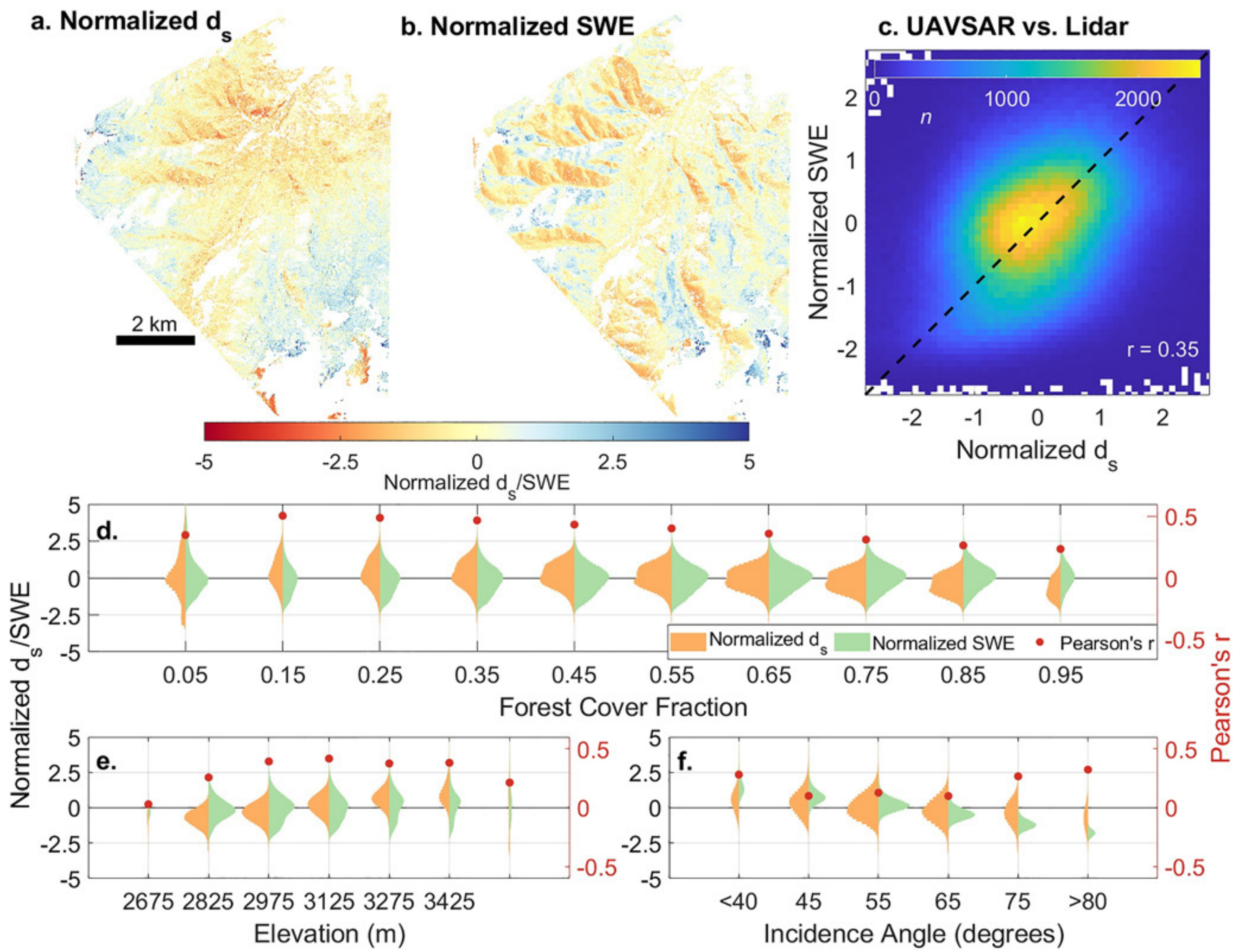

Figure 4. Normalized (a) lidar snow depth and (b) cumulative UAVSAR SWE, and (c) a 2-d histogram showing the comparison between the two (98% of points are shown). Violin plots showing the histogram distributions of normalized lidar snow depth and normalized UAVSAR SWE and r binned by (d) forest cover fraction, (e) elevation, and (f) UAVSAR incidence angle.

4.3. Normalized UAVSAR SWE Versus Normalized Lidar Snow Depth

Normalized UAVSAR SWE and normalized lidar depth yielded similar distribution patterns, particularly in the St. Louis Creek valley (trends SW to NE; Figures 4a and 4b) and near higher elevations (western and southern edges; Figures 4a and 4b). However, normalized UAVSAR SWE diverges from normalized lidar depths where SAR viewing geometries are complex (i.e., Figure 1b). Normalized depth/SWE have $r = 0.35$ (Figure 4c).

For FCF 0.10–0.60, mean normalized depths are greater than mean normalized SWE by 0.10–0.50 ($r = 0.40$–0.51), but for FCF > 0.60, mean normalized SWE are greater than mean normalized depths by 0.06–0.85 and correlation coefficients drop by ~0.04 per increase of 0.10 FCF (Figure 4d). Both normalized depth and SWE increase with increasing elevation, but the distributions are offset for elevations <2,900 m and >3,350 m (Figure 4e). The distribution of normalized SWE agreed well with normalized depth at incidence angles from 50 to 70° (Figure 4f), but yielded poor correlations ($r = 0.10$–0.13). Normalized SWE is biased positively for incidence angles <50° (mean = +0.58 normalized depth/SWE) and negatively for incidence angles >70° (mean = −0.85 normalized depth/SWE). Finally, mean normalized SWE was within ±0.08 of mean normalized depth for coherences of 0.30–0.70 (Figure S12 in Supporting Information S1). Correlation coefficients between each of the variables are presented in Table S7 in Supporting Information S1.

5. Discussion

5.1. Applications and Limitations of L-Band InSAR in Montane Forests

Forests challenge InSAR ΔSWE retrievals because trees attenuate the radar signal, and this effect increases as temperatures approach 0°C (Lemmetyinen et al., 2022). Additionally, tree sway due to wind and snow loading and shifts in the branches can influence the location of the phase-center (e.g., Raleigh et al., 2022), reducing coherence and confounding the interferometric snow signal. The accumulation of snow in the forest canopy, which is common in many snow climates, causes additional attenuation (Lemmetyinen et al., 2022). Snow in the canopy has different energy balance dynamics than snowpack below (Bonner et al., 2022), and may reduce coherence if the snow is wet. Recent tower-based, UAVSAR, and ALOS-2 studies suggest that L-band InSAR SWE retrievals may underestimate SWE by more than 50% in the forests at weekly or longer temporal baselines (Bonnell et al., 2024; Ruiz et al., 2022, 2024). In contrast, we found that SWE retrievals were only biased for FCF > 0.50, with in situ observations and normalized lidar yielding different ΔSWE retrieval biases (range = −21 to −16 mm ΔSWE vs. range = −0.11 to +0.80 normalized SWE). However, we note that <10% of in situ observations were obtained in FCF > 0.50 and recommend further evaluation in these environments.

It may be simpler to conclude that L-band InSAR is severely limited in heavily forested areas, but the polarimetric decomposition yields only slight differences between radar backscatter properties of any FCF interval >0.10 (Figure S11 in Supporting Information S1). The positive bias of normalized SWE relative to normalized snow depths at higher FCF might be explained by the presence of snow in the forest canopy, which can be included in the ΔSWE retrieval, whereas the lidar snow depth calculation removes the tree canopy. Based on field photographs and satellite imagery, we determined that canopy-intercepted snow was spatially extensive during the last three UAVSAR flights of March (Figure S4 in Supporting Information S1; Planet Labs PBC, 2021) and may have caused the positive bias for normalized SWE. Thus, determining the phase contributions from temperature-driven signal attenuation by trees and positional changes of scatterers caused by tree-sway/branch movement is a critical next step for L-band InSAR ΔSWE retrievals.

5.2. Implications for NISAR

The overall RMSE and correlation coefficients of the UAVSAR SWE retrievals, compared to in situ observations (RMSE = ∼18 mm; r = 0.55–0.65; Figures 3b and 3c; Tables S5–S8 in Supporting Information S1), fall within the range identified by previous UAVSAR studies (Bonnell et al., 2024; Hoppinen et al., 2024; Marshall et al., 2021; Tarricone et al., 2023). Here, we examine the utility of the L-band InSAR technique for operational SWE monitoring.

Single pair InSAR ΔSWE retrievals were relatively unbiased for FCF < 0.4 (Figures S9c, S10c in Supporting Information S1). Cumulative InSAR SWE was within 30 mm accuracy for StL, but increased to 50 mm accuracy for FC and HQ (Figure 3a), indicating L-band InSAR has the potential to meet the 30 mm absolute SWE accuracy goal set by the Decadal Survey (NASEM, 2018). The L-band InSAR technique will have three distinct advantages: (a) global coverage from NISAR that is (b) repeated every 12 days and (c) does not require any density modeling in dry snowpacks (e.g., Leinss et al., 2015; Oveisgharan et al., 2024). Considering that current global reanalysis products underestimate SWE by as much as 70% and poorly represent SWE distributions (Broxton et al., 2016), the L-band InSAR technique offers a significant step in the right direction.

Operational ΔSWE retrievals from NISAR will be challenged by many factors. Similar to previous studies (Bonnell et al., 2024; Tarricone et al., 2023), we found that ΔSWE retrievals can be obtained at lower coherences (<0.4), albeit with reduced accuracy (RMSE = 30–40 mm; Figure 3d). Low coherence causes phase unwrapping errors, which can be addressed through filtering techniques (e.g., Lei et al., 2023) or by using wrapped phase products (e.g., Hoppinen et al., 2024; Oveisgharan et al., 2024). Atmospheric and ionospheric corrections will be released with NISAR interferograms, but previous studies have shown that the atmospheric corrections will need to be evaluated (Kirui et al., 2021) and that large phase-change contributions from the ionosphere can significantly hinder accurate ΔSWE retrievals (Ruiz et al., 2024). Wet snow remains a challenging problem for radar SWE retrievals because liquid water causes signal attenuation that can result in overestimation of ΔSWE (Bonnell et al., 2021; Hoppinen et al., 2024; Tarricone et al., 2023) or complete decorrelation of the radar signal (Ruiz et al., 2022), but it may be possible to develop a NISAR approach to identify the presence of liquid water in the snowpack (e.g., Gagliano et al., 2023; Lund et al., 2022; Park et al., 2014). Finally, we used a lidar DEM to calculate UAVSAR incidence angles because the leading global DEM (Copernicus DEM) was generated from high-frequency InSAR, which has limited canopy penetration (Gdulová et al., 2020). This will likely add uncertainty for forest snowpack monitoring.

6. Conclusion

The need for global snowpack monitoring is greater than ever (Hale et al., 2023; Siirila-Woodburn et al., 2021), but nearly all snow remote sensing methods are challenged by forest cover. Recent studies support the use of the upcoming L-band NISAR satellite for global SWE retrievals at high spatiotemporal resolution, and it may be viable as soon as the 2025 southern hemisphere winter. Previous work suggested that L-band InSAR ΔSWE retrievals may be hindered significantly by forest cover (e.g., Ruiz et al., 2022), but we found the technique to be accurate in FCF < 0.50 (RMSEs = 14–26 mm; Figure 3f) across the 10 week NASA SnowEx 2021 campaign at FEF in Colorado. We identified strong similarities between the spatial distributions of normalized lidar snow depths and normalized UAVSAR SWE, although the pixel-wise Pearson's correlation coefficient was relatively low ($r = 0.35$; Figure 4). Critically, comparisons against normalized lidar snow depths and in situ measurements support the technique's use in FCF < 0.50, but further research is necessary to determine whether uncertainties in FCF > 0.50 are within the acceptable limits for operational use. Thus, NISAR may be feasible for snowpack monitoring in sparse to moderate forest cover, which would vastly increase the global applicability of this method.

Data Availability Statement

UAVSAR InSAR pair and POLSAR data sets are available at NASA UAVSAR (2021; https://doi.org/10.5067/7PEQV8SVR4DM) and the look vectors are available at NASA UAVSAR (2023; https://uavsar.jpl.nasa.gov/cgi-bin/product.pl?jobName=fraser_05209_21021_003_210322_L090_CX_01#data). Lidar data sets for snow depth, vegetation height, and digital elevation model are available at Adebisi et al. (2022a, 2022b, 2022c). Snow pits are archived at the NSIDC (Mason et al., 2024) and probed depths are under review at the NSIDC. Fool Creek SNOTEL data are available at USDA (2024; https://wcc.sc.egov.usda.gov/nwcc/site?sitenum=1186). UAVSAR ΔSWE products are archived with Dryad (https://doi.org/10.5061/dryad.x3ffbg7tg) during the review process and will be released publicly, pending the review of our manuscript.

Acknowledgments
R.B. acknowledges NASA FINESST award 80NSSC20K1624. K.E. and B.S. acknowledge NASA award NNG210B37A. D.M. and H.P.M. acknowledge NASA awards 80NSSC18K1405 and 80NSSC22K1113. H.P.M. acknowledges CRREL contract number W913E5-24-C-0015. We thank the NASA SnowEx leadership team for implementing the 2021 Time Series Campaign and M. Mason for archiving support. We thank the NASA UAVSAR team for collecting and processing UAVSAR data sets. We acknowledge the field efforts of S. Kinney and D. Craaybeek. Finally, we thank two anonymous reviewers for their comments and suggestions that improved our study.

References

Adebisi, N., Marshall, H., O'Neel, S., Vuyovich, C. M., Hiemstra, C., & Elder, K. (2022a). SnowEx20-21 QSI lidar DEM 0.5m UTM grid, version 1 [Dataset]. *Boulder, Colorado USA. NASA National Snow and Ice Data Center Distributed Active Archive Center*. https://doi.org/10.5067/YO583L7ZOLOO

Adebisi, N., Marshall, H., Vuyovich, C. M., Elder, K., Hiemstra, C., & Durand, M. (2022b). SnowEx20-21 QSI lidar snow depth 0.5m UTM grid, version 1 [Dataset]. *Boulder, Colorado USA. NASA National Snow and Ice Data Center Distributed Active Archive Center*. https://doi.org/10.5067/VBUN16K365DG

Adebisi, N., Marshall, H., Vuyovich, C. M., Elder, K., Hiemstra, C., & Durand, M. (2022c). SnowEx20-21 QSI lidar vegetation height 0.5m UTM grid, version 1 [Dataset]. *Boulder, Colorado USA. NASA National Snow and Ice Data Center Distributed Active Archive Center*. https://doi.org/10.5067/8RBIUIPEUJ7Z

Alexander, R., & Watkins, R. (1977). *The Fraser Experimental Forest* (p. 39). USDA Forest Service.

Barnett, T. P., Adam, J. C., & Lettenmaier, D. P. (2005). Potential impacts of a warming climate on water availability in snow-dominated regions. *Nature*, *438*(7066), 7066–7309. https://doi.org/10.1038/nature04141

Bevis, M., Businger, S., Herring, T. A., Rocken, C., Anthes, R. A., & Ware, R. H. (1992). GPS meteorology: Remote sensing of atmospheric water vapor using the global positioning system. *Journal of Geophysical Research*, *97*(D14), 15787–15801. https://doi.org/10.1029/92JD01517

Bonnell, R., McGrath, D., Tarricone, J., Marshall, H. P., Bump, E., Duncan, C., et al. (2024). Evaluating L-band InSAR snow water equivalent retrievals with repeat ground-penetrating radar and terrestrial lidar surveys in northern Colorado. *EGUsphere [preprint]*, 1–33. https://doi.org/10.5194/egusphere-2024-236

Bonnell, R., McGrath, D., Williams, K., Webb, R., Fassnacht, S. R., & Marshall, H.-P. (2021). Spatiotemporal variations in liquid water content in a seasonal snowpack: Implications for radar remote sensing. *Remote Sensing*, *13*(21), 21. https://doi.org/10.3390/rs13214223

Bonner, H. M., Raleigh, M. S., & Small, E. E. (2022). Isolating forest process effects on modelled snowpack density and snow water equivalent. *Hydrological Processes*, *36*(1), e14475. https://doi.org/10.1002/hyp.14475

Bourgoin, C., Ameztoy, I., Verhegghen, A., Carboni, S., Colditz, R. R., & Achard, F. (2023). Global map of forest cover 2020 - Version 1 [Dataset]. *European Commission, Joint Research Center*. http://data.europa.eu/89h/10d1b337-b7d1-4938-a048-686c8185b290

Broxton, P. D., Zeng, X., & Dawson, N. (2016). Why do global reanalyses and land data assimilation products underestimate snow water equivalent? *Journal of Hydrometeorology*, *17*(11), 2743–2761. https://doi.org/10.1175/JHM-D-16-0056.1

Cloude, S. R., & Pottier, E. (1997). An entropy based classification scheme for land applications of polarimetric SAR. *IEEE Transactions on Geoscience and Remote Sensing*, *35*(1), 68–78. https://doi.org/10.1109/36.551935

Conde, V., Nico, G., Mateus, P., Catalão, J., Kontu, A., & Gritsevich, M. (2019). On the estimation of temporal changes of snow water equivalent by spaceborne sar interferometry: A new application for the Sentinel-1 mission. *Journal of Hydrology and Hydromechanics*, *67*(1), 93–100. https://doi.org/10.2478/johh-2018-0003

Deeb, E. J., Forster, R. R., & Kane, D. L. (2011). Monitoring snowpack evolution using interferometric synthetic aperture radar on the North Slope of Alaska, USA. *International Journal of Remote Sensing*, *32*(14), 3985–4003. https://doi.org/10.1080/01431161003801351

Di Paolo, F., Cosciotti, B., Lauro, S. E., Mattei, E., & Pettinelli, E. (2020). A critical analysis on the uncertainty computation in ground-penetrating radar-retrieved dry snow parameters. *Geophysics*, *85*(4), H39–H49. https://doi.org/10.1190/geo2019-0683.1

Doin, M. P., Lasserre, C., Peltzer, G., Cavalié, O., & Doubre, C. (2009). Corrections of stratified tropospheric delays in SAR interferometry: Validation with global atmospheric models. *Journal of Applied Geophysics*, *69*(1), 35–50. https://doi.org/10.1016/j.jappgeo.2009.03.010

Dozier, J., Bair, E. H., & Davis, R. E. (2016). Estimating the spatial distribution of snow water equivalent in the world's mountains. *WIREs Water*, *3*(3), 461–474. https://doi.org/10.1002/wat2.1140

Elder, K., Cline, D., Liston, G. E., & Armstrong, R. (2009). NASA Cold Land Processes Experiment (CLPX 2002/03): Field measurements of snowpack properties and soil moisture. *Journal of Hydrometeorology*, *10*(1), 320–329. https://doi.org/10.1175/2008JHM877.1

Eppler, J., Rabus, B., & Morse, P. (2022). Snow water equivalent change mapping from slope-correlated synthetic aperture radar interferometry (InSAR) phase variations. *The Cryosphere*, *16*(4), 1497–1521. https://doi.org/10.5194/tc-16-1497-2022

Gagliano, E., Shean, D., Henderson, S., & Vanderwilt, S. (2023). Capturing the onset of mountain snowmelt runoff using satellite synthetic aperture radar. *Geophysical Research Letters*, *50*(21), e2023GL105303. https://doi.org/10.1029/2023GL105303

Gdulová, K., Marešová, J., & Moudrý, V. (2020). Accuracy assessment of the global TanDEM-X digital elevation model in a mountain environment. *Remote Sensing of Environment*, *241*, 111724. https://doi.org/10.1016/j.rse.2020.111724

Gleason, K. E., Bradford, J. B., D'Amato, A. W., Fraver, S., Palik, B. J., & Battaglia, M. A. (2021). Forest density intensifies the importance of snowpack to growth in water-limited pine forests. *Ecological Applications*, *31*(1), e02211. https://doi.org/10.1002/eap.2211

Gong, W., Meyer, F. J., Webley, P., & Morton, D. (2013). Performance of the high-resolution atmospheric model HRRR-AK for correcting geodetic observations from spaceborne radars. *Journal of Geophysical Research: Atmospheres*, *118*(20), 11611–11624. https://doi.org/10.1002/2013JD020170

Greene, E., Birkeland, K., Elder, K., McCammon, I., Staples, M., Sharaf, D., et al. (2022). *Snow, weather, and avalanches: Observation guidelines for avalanche programs in the United States* (4th ed.). American Avalanche Association.

Guneriussen, T., Hogda, K. A., Johnsen, H., & Lauknes, I. (2001). InSAR for estimation of changes in snow water equivalent of dry snow. *IEEE Transactions on Geoscience and Remote Sensing*, *39*(10), 2101–2108. https://doi.org/10.1109/36.957273

Hale, K. E., Jennings, K. S., Musselman, K. N., Livneh, B., & Molotch, N. P. (2023). Recent decreases in snow water storage in western North America. *Communications Earth & Environment*, *4*(1), 1. https://doi.org/10.1038/s43247-023-00751-3

Hoppinen, Z., Oveisgharan, S., Marshall, H.-P., Mower, R., Elder, K., & Vuyovich, C. (2024). Snow water equivalent retrieval over Idaho - Part 2: Using L-band UAVSAR repeat-pass interferometry. *The Cryosphere*, *18*(2), 575–592. https://doi.org/10.5194/tc-18-575-2024

Hoppinen, Z., & Tarricone, J. (2022). uavsar_pytools Version 0.7.0 [code]. *Zenodo*. https://doi.org/10.5281/zenodo.6789624

Hu, J. M., Shean, D., & Bhushan, S. (2023). Six consecutive seasons of high-resolution mountain snow depth maps from satellite stereo imagery. *Geophysical Research Letters*, *50*(24), e2023GL104871. https://doi.org/10.1029/2023GL104871

Huckaby, L. S., & Moir, W. H. (1998). Forest communities at Fraser Experimental Forest, Colorado. *Southwestern Naturalist*, *43*(2), 204–218. https://www.jstor.org/stable/30055357

Immerzeel, W. W., Lutz, A. F., Andrade, M., Bahl, A., Biemans, H., Bolch, T., et al. (2020). Importance and vulnerability of the world's water towers. *Nature*, *577*(7790), 364–369. https://doi.org/10.1038/s41586-019-1822-y

Jonas, T., Marty, C., & Magnusson, J. (2009). Estimating the snow water equivalent from snow depth measurements in the Swiss Alps. *Journal of Hydrology*, *378*(1), 161–167. https://doi.org/10.1016/j.jhydrol.2009.09.021

Kirui, P. K., Reinosch, E., Isya, N., Riedel, B., & Gerke, M. (2021). Mitigation of atmospheric artefacts in multi temporal InSAR: A review. *PFG – Journal of Photogrammetry, Remote Sensing and Geoinformation Science*, *89*(3), 251–272. https://doi.org/10.1007/s41064-021-00138-z

Kovacs, A., Gow, A. J., & Morey, R. M. (1995). The in-situ dielectric constant of polar firn revisited. *Cold Regions Science and Technology*, *23*(3), 245–256. https://doi.org/10.1016/0165-232X(94)00016-Q

Lei, Y., Shi, J., Liang, C., Werner, C., & Siqueira, P. (2023). Snow water equivalent retrieval using spaceborne repeat-pass L-band SAR interferometry over sparse vegetation covered regions. *IGARSS 2023 - 2023 IEEE International Geoscience and Remote Sensing Symposium*, 852–855. https://doi.org/10.1109/IGARSS52108.2023.10282234

Leinss, S., Wiesmann, A., Lemmetyinen, J., & Hajnsek, I. (2015). Snow water equivalent of dry snow measured by differential interferometry. *Ieee Journal of Selected Topics in Applied Earth Observations and Remote Sensing*, *8*(8), 3773–3790. https://doi.org/10.1109/JSTARS.2015.2432031

Lemmetyinen, J., Ruiz, J. J., Cohen, J., Haapamaa, J., Kontu, A., Pulliainen, J., & Praks, J. (2022). Attenuation of radar signal by a boreal forest canopy in winter. *IEEE Geoscience and Remote Sensing Letters*, *19*, 1–5. https://doi.org/10.1109/LGRS.2022.3187295

Li, D., Wrzesien, M. L., Durand, M., Adam, J., & Lettenmaier, D. P. (2017). How much runoff originates as snow in the western United States, and how will that change in the future? *Geophysical Research Letters*, *44*(12), 6163–6172. https://doi.org/10.1002/2017GL073551

Li, Y., Zhao, X., & Zhao, Q. (2022). Snow depth inversion in forest areas from sentinel-1 data based on phase deviation correction. *Remote Sensing*, *14*(23), 23. https://doi.org/10.3390/rs14235930

Lievens, H., Demuzere, M., Marshall, H.-P., Reichle, R. H., Brucker, L., Brangers, I., et al. (2019). Snow depth variability in the Northern Hemisphere mountains observed from space. *Nature Communications*, *10*(1), 1. https://doi.org/10.1038/s41467-019-12566-y

Livneh, B., & Badger, A. M. (2020). Drought less predictable under declining future snowpack. *Nature Climate Change*, *10*(5), 5–458. https://doi.org/10.1038/s41558-020-0754-8

Lund, J., Forster, R. R., Deeb, E. J., Liston, G. E., Skiles, S. M., & Marshall, H.-P. (2022). Interpreting sentinel-1 SAR backscatter signals of snowpack surface melt/freeze, warming, and ripening, through field measurements and physically-based SnowModel. *Remote Sensing*, *14*(16), 16. https://doi.org/10.3390/rs14164002

Marshall, H. P., Deeb, E., Forster, R., Vuyovich, C., Elder, K., Hiemstra, C., & Lund, J. (2021). L-band InSAR depth retrieval during the NASA SnowEx 2020 campaign: Grand Mesa, Colorado. *2021 IEEE International Geoscience and Remote Sensing Symposium IGARSS*, 625–627. https://doi.org/10.1109/IGARSS47720.2021.9553852

Marshall, H. P., Vuyovich, C., Skiles, M., Sproles, E., Gleason, K., & Elder, K. (2020). NASA SnowEx 2021 experiment plan [science plan]. https://snow.nasa.gov/sites/default/files/users/user194/NASASnowEx21_ExperimentPlan_draft_v02.pdf

Mason, M., Marshall, H., Craaybeek, D., Elder, K., & Vuyovich, C. M. (2024). SnowEx21 time series snow pits, version 1 [Dataset]. *Boulder, Colorado USA. NASA National Snow and Ice Data Center Distributed Active Archive Center*. https://doi.org/10.5067/QIANJYJGRWOV

Michaelides, R. J., Chen, R. H., Zhao, Y., Schaefer, K., Parsekian, A. D., Sullivan, T., et al. (2021). Permafrost dynamics observatory—Part I: Postprocessing and calibration methods of UAVSAR L-band InSAR data for seasonal subsidence estimation. *Earth and Space Science*, *8*(7), e2020EA001630. https://doi.org/10.1029/2020EA001630

Moore, C., Kampf, S., Stone, B., & Richer, E. (2012). Snow persistence grids and snow zone shape files for the western United States [Dataset]. *Mountain Scholar*. https://doi.org/10.25675/10217/171907

Nagler, T., Rott, H., Scheiblauer, S., Libert, L., Mölg, N., Horn, R., et al. (2022). Airborne experiment on InSAR snow mass retrieval in alpine environment. *IGARSS 2022 - 2022 IEEE International Geoscience and Remote Sensing Symposium*, 4549–4552. https://doi.org/10.1109/IGARSS46834.2022.9883809

NASA SnowEx. (2024). SnowEx [website]. *NASA Snow*. Retrieved from https://snow.nasa.gov/campaigns/snowex. Accessed 5 April 2024.

NASA UAVSAR. (2021). POLSAR and repeat pass InSAR pair products for Fraser, Colorado flight line [Dataset]. *Alaska Satellite Facility Distributed Active Archive Center*. https://doi.org/10.5067/7PEQV8SVR4DM

NASA UAVSAR. (2023). Product: Fraser_05209_21021_003_210322_L090_CX01, coregistered SLC stack of Fraser, Colorado [Dataset]. *NASA Jet Propulsion Laboratory*. Retrieved from https://uavsar.jpl.nasa.gov/cgi-bin/product.pl?jobName=fraser_05209_21021_003_210322_L090_CX_01#data

NASEM, National Academies of Sciences, Engineering, and Medicine. (2018). *Thriving on our changing Planet: A decadal strategy for Earth observation from space*. National Academies Press. https://doi.org/10.17226/24938

Nielsen, A. A. (2022). The eigenvector-eigenvalue identity applied to fast calculation of polSAR scattering characterization. *IEEE Geoscience and Remote Sensing Letters*, *19*, 1–5. https://doi.org/10.1109/LGRS.2022.3169994

Oveisgharan, S., Zinke, R., Hoppinen, Z., & Marshall, H. P. (2024). Snow water equivalent retrieval over Idaho - Part 1: Using sentinel-1 repeat-pass interferometry. *The Cryosphere*, *18*(2), 559–574. https://doi.org/10.5194/tc-18-559-2024

Palomaki, R. T., & Sproles, E. A. (2023). Assessment of L-band InSAR snow estimation techniques over a shallow, heterogeneous prairie snowpack. *Remote Sensing of Environment*, *296*, 113744. https://doi.org/10.1016/j.rse.2023.113744

Park, S.-E., Yamaguchi, Y., Singh, G., Yamaguchi, S., & Whitaker, A. C. (2014). Polarimetric SAR response of snow-covered area observed by multi-temporal ALOS PALSAR fully polarimetric mode. *IEEE Transactions on Geoscience and Remote Sensing*, *52*(1), 329–340. https://doi.org/10.1109/TGRS.2013.2240000

Pedersen, S. H., Bentzen, T. W., Reinking, A. K., Liston, G. E., Elder, K., Lenart, E. A., et al. (2021). Quantifying effects of snow depth on caribou winter range selection and movement in Arctic Alaska. *Movement Ecology*, *9*(1), 48. https://doi.org/10.1186/s40462-021-00276-4

Planet Labs PBC. (2021). *Planet application program interface: In space for life on Earth*. Planet. Retrieved from https://api.planet.com

Raleigh, M. S., Gutmann, E. D., Van Stan, J. T., Burns, S. P., Blanken, P. D., & Small, E. E. (2022). Challenges and capabilities in estimating snow mass intercepted in conifer canopies with tree sway monitoring. *Water Resources Research*, *58*(3), e2021WR030972. https://doi.org/10.1029/2021WR030972

Ruiz, J., Merkouriadi, I., Lemmetyinen, J., Cohen, J., Kontu, A., Nagler, T., et al. (2024). Comparing InSAR snow water equivalent retrieval using ALOS2 with in situ observations and SnowModel over the boreal forest area. *IEEE Transactions on Geoscience and Remote Sensing*, *62*, 1–14. https://doi.org/10.1109/TGRS.2024.3439855

Ruiz, J. J., Lemmetyinen, J., Kontu, A., Tarvainen, R., Vehmas, R., Pulliainen, J., & Praks, J. (2022). Investigation of environmental effects on coherence loss in SAR interferometry for snow water equivalent retrieval. *IEEE Transactions on Geoscience and Remote Sensing*, *60*, 1–15. https://doi.org/10.1109/TGRS.2022.3223760

Siirila-Woodburn, E. R., Rhoades, A. M., Hatchett, B. J., Huning, L. S., Szinai, J., Tague, C., et al. (2021). A low-to-no snow future and its impacts on water resources in the western United States. *Nature Reviews Earth and Environment*, *2*(11), 11–819. https://doi.org/10.1038/s43017-021-00219-y

Sturm, M., Goldstein, M. A., & Parr, C. (2017). Water and life from snow: A trillion dollar science question. *Water Resources Research*, *53*(5), 3534–3544. https://doi.org/10.1002/2017WR020840

Tarricone, J., Webb, R. W., Marshall, H.-P., Nolin, A. W., & Meyer, F. J. (2023). Estimating snow accumulation and ablation with L-band interferometric synthetic aperture radar (InSAR). *The Cryosphere*, *17*(5), 1997–2019. https://doi.org/10.5194/tc-17-1997-2023

Trujillo, E., & Molotch, N. P. (2014). Snowpack regimes of the western United States. *Water Resources Research*, *50*(7), 5611–5623. https://doi.org/10.1002/2013WR014753

Tsang, L., Durand, M., Derksen, C., Barros, A. P., Kang, D.-H., Lievens, H., et al. (2022). Review article: Global monitoring of snow water equivalent using high-frequency radar remote sensing. *The Cryosphere*, *16*(9), 3531–3573. https://doi.org/10.5194/tc-16-3531-2022

USDA. (2024). Fool Creek, USDA Natural Resources Conservation Service [Dataset]. Retrieved from https://wcc.sc.egov.usda.gov/nwcc/site?sitenum=1186

Wrzesien, M. L., Durand, M. T., Pavelsky, T. M., Kapnick, S. B., Zhang, Y., Guo, J., & Shum, C. K. (2018). A new estimate of North American mountain snow accumulation from regional climate model simulations. *Geophysical Research Letters*, *45*(3), 1423–1432. https://doi.org/10.1002/2017GL076664